UHF RFID Wristbands: A Long-Range, Durable, Flexible, and Low-Cost Tag Antenna Design

Sergio López-Soriano, Joan Melià-Seguí, *Senior Member, IEEE*, and Josep Parrón Granados

***Abstract*—This contribution is focused on the performance evaluation of a long-range patch-type antenna for ultra-high frequency (UHF) radiofrequency identification (RFID) wristband tags. The antenna design was presented in the IEEE International Conference on RFID Technology and Applications (RFID-TA), held on September 4-6, 2023, Aveiro, Portugal, under the title "A durable and flexible, low-cost tag antenna design for UHF RFID wearable applications". First, the theoretical and practical evaluation of the wristband tag antenna is conducted in four different scenarios. Next, the studied solution is benchmarked against a selection of the current commercial solutions. The proposed antenna design is mounted on a flexible and low-cost Teflon (PTFE) substrate, and it consists of a disconnected metal-substrate-metal layered structure. To produce a light and comfortable wearable device, the wristband design constraints limit the thickness to 1 mm and the width to 3 cm. The design is intended to be used in human identification and tracking applications while providing enough durability to endure for a prolonged period without significant antenna de-tuning. The proposed wristband is designed to operate in the FCC band (902-928 MHz) and it can reach distances over 3-5 meters, depending on the microchip sensitivity. The results of the experiments show that the performance of the proposed wristband design is comparable to current commercial solutions, while offering a different set of features. A discussion on the comparison between the current solutions and the proposed wristband antenna is provided in the text.**

***Index Terms*—RFID, wristband, long-range, patch antenna, flexible.**

I. Introduction

RADIO-FREQUENCY identification (RFID), technology has become an integral part of various industries, offering seamless identification, tracking and sensing capabilities [1], [2], [3], [4]. Ultra-High Frequency (UHF) RFID tags stand out for their long-range communication and high data transfer rates. Furthermore, over the past decade, the application of RFID tags integrated into wristbands for human identification and tracking has garnered significant attention from both the scientific community and industry.

Typical applications comprise access control, ticketing, personnel tracking and asset management in diverse environments [5], [6], [7], [8]. In all cases, the tag antenna design plays a pivotal role in the performance of the wristbands. Therefore, optimizing the design of the antenna can lead to substantial improvements in read range (*Rr*), accuracy, and overall system reliability. In addition, wristband antenna designs face distinct constraints specific of the target applications, primarily revolving around antenna geometry and dimensions.

In response to these challenges, numerous contributions have proposed different solutions [9], [10], [11], [12], [13], [14], [15], [16], [17], [18]. However, while wristband designs documented in the literature generally offer reasonable read ranges ranging from 2 to 3 meters and over [9], [10], [11], [12], [13], [14], [15], the current solutions still present limitations in terms of flexibility, cost-effectiveness, durability, and extended range ([13], [15], [19], [20]).

Moreover, UHF RFID wristbands have entered the commercial market in various formats [16], [17], [18]. These commercial wristbands can be categorized into two groups based on the cover material: rubber bands [16] and thermal paper wristbands [17], [18]. Thermal paper wristbands typically feature cost-effective ultra-thin flexible designs utilizing meander line antennas (MLAs), boasting read ranges of up to 17 meters. However, the radiation efficiency of these designs is significantly impacted by the proximity of high-loss materials such as metals or the human body. Additionally, these devices prove suboptimal for harsh environments where tags may be prone to bending and breakage. On the other hand, rubber bands [16] that incorporate dipole and patch antennas are more durable, achieving read ranges of up to 5 meters. Nevertheless, these wristbands come with a higher cost, in the order of a few euros (1-4 €).

This contribution assesses the performance of a new wristband design consisting of a low-cost, thin and flexible antenna for UHF RFID wristbands [21]. The design involves two open-ended coupled patch antennas connected by the RFID integrated circuit (IC). To the best of the authors' knowledge, this antenna configuration hasn't been previously documented in the literature and it contributes to the state of the art of

Manuscript received 24 November 2023; revised 12 January 2024; accepted 6 February 2024. Date of publication 14 February 2024; date of current version 7 May 2024. This work was supported in part by the Spanish Ministry of Culture and Sports; in part by the European Funds for the Recovery, Transformation and Resilience Plan through HydraSport Project under Grant EXP_75087; in part by the Spanish Ministry of Science, Innovation and Universities through RF-VOLUTION Project under Grant PID2021-122247OB-I00 and through MATILDE Project under Grant PID2021-127203OB-I00; and in part by the Generalitat de Catalunya through Suport a Grups de Recerca (SGR) Funds under Grant 2021-SGR-00174. *(Corresponding author: S. López-Soriano.)*

Sergio López-Soriano is with the Internet Interdisciplinary Institute, Universitat Oberta de Catalunya, 08035 Barcelona, Spain (e-mail: slopezsor@uoc.edu).

Joan Melià-Seguí is with the Faculty of Computer Science, Multimedia and Telecommunication, Universitat Oberta de Catalunya, 08035 Barcelona, Spain (e-mail: melia@uoc.edu).

Josep Parrón Granados is with the Departament de Telecomunicació i Enginyeria de Sistemes, Universitat Autònoma de Barcelona, 08193 Bellaterra, Spain (e-mail: josep.parron@uab.cat).

Digital Object Identifier 10.1109/JRFID.2024.3365796

RFID tag antennas by providing a flexible and durable solution while attaining higher read ranges, at the expense of having a larger antenna footprint.

In this document, the presented prototype will be compared to the most recent state of the art and benchmarked against the current top-tier commercial products, seeking to establish optimal conditions for comparability. The comparative evaluation aims to highlight the relative strengths and limitations, providing a comprehensive view of the performance of the proposed design in relation to existing commercial solutions.

The document is organized as follows: Section II presents a review of the state of the art. Section III describes the wristband antenna design proposed in [21]. Section IV contains the performance analysis of the wristband in four different scenarios. In Section V, the wristband performance is compared to a selection of commercial wristbands. Finally, Section VI provides the conclusions of this work.

II. State of the Art

Wristband antenna designs can be classified through different categories: antenna type, number of layers, manufacturing materials, wristband length, wristband width, wristband thickness, flexibility and read range. Table I summarizes the available information about the most relevant designs found in a thorough review of the state of the art and the available commercial solutions. In a first classification, we distinguish wristband designs with one metallic layer [13], [15] and designs using two, top and bottom, metallic layers [9], [10], [11], [12], [14].

Designs with a single conductive layer produce thinner wristbands. Instead, they attain lower read ranges due to the direct interaction of the electric field with the human arm. An example of this wristband type is presented in [13], where the wristband is fabricated with a 3D printing pen. The substrate consists of a flexible plastic material and the loop antenna is fabricated using a conductive thread. However, the read range is just 50 cm. Therefore, it is not well suited for many applications. In [15], a meandered dipole is loaded with metamaterial inspired structures. The read range is not provided in this contribution, but it has been calculated from the realized gain (Table I). The wristband attains 2.9 meters of read range at the cost of a large antenna size.

Designs including two metallic layers are the most common in the literature due to the isolation provided by the bottom layer to reduce the radiation absorbed by the human body. The designs presented in [9], [12] can be analyzed as radiating slots [22] opened in the middle of two short-ended parallel plate transmission lines [23]. In [9], a bow tie shape is used to improve the tag bandwidth and two slots are opened close to the shorted ends of the antenna to increase the antenna electrical length. The design presented in [12] is an evolution of [9]. The rigid part of the wristband has been reduced by integrating a flexible plastic material in the antenna substrate. The length of these symmetrical designs can be reduced to the half, resulting in a planar inverted-F antenna (PIFA) design. An example of this technique is presented in [10] (Fig. 1a), where a thin strip connects the IC to the bottom conductor at the symmetry plane. Additionally, a post-fabrication tunning mechanism is used to provide impedance matching to different ICs.

The research conducted in [11] also exploits the concept of using a wide metallic strip at the bottom of the wristband to isolate the tag from the human arm, but in this case the antenna consists of a normal mode helical antenna (NMHA). The proposed prototype achieves very small footprint at the expense of increasing its thickness. Therefore, even if the antenna is built on a rigid substrate, the wristband is almost completely flexible. A rigid and thick bracelet including a PIFA antenna is proposed in [14]. This design attains a high read range. However, its size and rigidity make it uncomfortable to wear and, therefore, unpractical for most applications.

On the other hand, a wide range of identification bracelets that use UHF RFID technology are currently being marketed [16] with different shapes and sizes. These designs attain fair read ranges while producing comfortable wristbands at different costs ranging from prices below 1 USD (Fig. 1e) to few dollars (Fig. 1f). In Fig. 1e, a dipole-like antenna is embedded in a silicone wristband implementing a structure for separating the tag antenna from the human arm to improve the antenna radiation. The antenna in Fig. 1f consists of a patch antenna mounted on a ceramic substrate. Using a high permittivity and low loss ceramic material allows, on the one side, miniaturizing the patch antenna while maximizing the radiation efficiency. The drawbacks are the high material cost and the bandwidth reduction. The final tag design is also embedded into a soft silicone material and the wristband attains fair read ranges of 3 to 5 meters in the U.S. frequency band (902 – 928 MHz).

The leading companies in the RFID industry are opting for solutions that prioritize comfort, simplicity and cost [17], [18]. These solutions are based on half-wave meandered line dipole antennas, with capacitive tip loading, fed through a T-match loop to match the antenna input impedance to the complex impedance of the RFID IC. However, in this application, the capacitive tip loading fulfills a rather important purpose. These designs are asymmetrical to allow different currents densities at both arms. They have a large capacitive tip at one antenna end, whose purpose is to scatter the currents flowing through the antenna along its surface. Therefore, this part is less sensitive to the effects produced by nearby high permittivity and high loss dielectric materials.

The same concept has been exploited, recently, in applications such as tagging of metallic objects [24], where a large capacitive tip can be stuck to the metallic object like a “flag”. In the case of UHF RFID wristbands, the whole antenna is left dangling from the wrist to provide further decoupling from the human arm/body. Wristband manufacturers state that their solutions [17], [18] attain read ranges of 2 meters when used in patients arms, which are considerably improved when they are measured in free space. Regarding the bracelet itself, these wristbands are ultra-thin, flexible, and very comfortable to wear. They are made of an antimicrobial synthetic polypropylene material. In addition, they are printable, which allows the

TABLE I
UHF RFID WRISTBAND ANTENNAS

Ref.	Antenna Type	Materials	IC name and sensitivity (dBm)		Size (mm)			Flexible	Read range (m)	Expected Rr (m)***
					L	*W*	*H*			
[9]	Slot	ARLON AD1000	Alien Higgs 3	−18	51.1	21.3	0.64	No	2.1	3.7
[10]	PIFA	ARLON AD1000	Alien Higgs 3	−18	36.3	27	0.64	No	2.2	3.9
[11]	NMHA	FR4 and PET	Alien Higgs 3	−18	26	8	1.65	No	> 2	3.5
[12]	Slot	FR4 + flexible PVC	Alien Higgs 4	−20.5	34	25	1.6	No	3	4
[13]	Loop	Bisphenol A (BPA) free plastic	NXP UCODE G2iL	−18	100	20	NA	Yes	≥ 0.5	0.9
[14]	PIFA	$\varepsilon_r = 5$ $\tan(\delta) = 0.02$	Impinj Monza 3	−15	76.4	14.2	3.5	No	3.8[1]	9.5
[15]	dipole	$\varepsilon_r = 3.2$ $\tan(\delta) = 0.05$	NXP SL3S1213 UCODE G2iL	−18	117	26	0.277	Yes	2.9[2]	5.1
[16][3]	dipole	NA	Monza R6-P	−22	106	6	5*	Yes	3 - 5**	3.3 - 5.6
[16][4]	patch	NA (Ceramic)	Monza R6-P	−22	25	25	3	No	3 - 5**	3.3 - 5.6
[17]	dipole	Polypropylene	NXP Ucode 8	−23	56	29	< 0.5	Yes	2 - 10**	2 - 10**
[18][5]	dipole	NA	BT0600	−23	40	15	< 0.5	Yes	< 3**	< 3**
[18][6]	dipole	NA	ZBR2002	−23	60	20	< 0.5	Yes	2 - 17**	2 - 17**
This work	patch	Teflon (PTFE)	Alien Higgs 4	−20.5	220	30	1	Yes	4.5 - 8	3 - 10.8

[1]calculated from the tag sensitivity [14], [2]calculated from Gτ, [3]TJNFCTAG TRSB03-001, [4]TJNFCTAG TRSB03-002, [5]Z-Band Direct, [6]Z-Band UltraSoft.
*Silicone spacer.
**Information retrieved from the manufacturer datasheet.
***Expected read range computed for microchip sensitivity of −23 dBm

(a) [10]

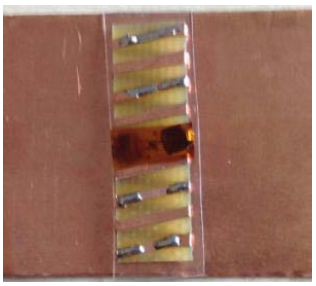

(b) [11][a] (© [2017] IEEE)

(c) [12]

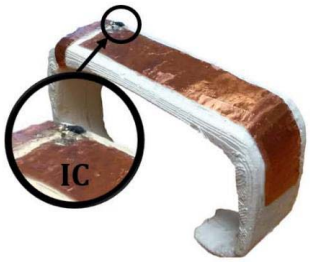

(d) [14][a] (© [2020] IEEE)

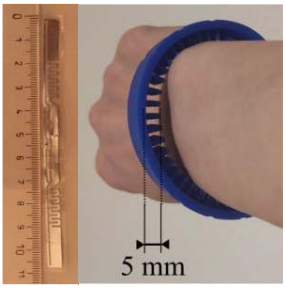

(e) [16][3]

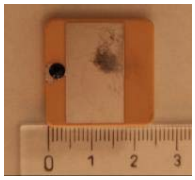

(f) [16][4]

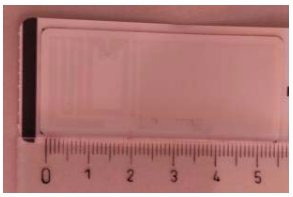

(g) [17]

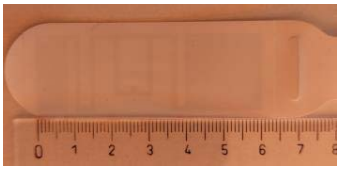

(h) [18][6]

Fig. 1. Images of wristband antenna designs corresponding to different antenna types found in the literature and the industry. [a] These images are reproduced with permission from the IEEE.

hospital to print QR codes or patient information for visual identification. These wristbands contain tag inlays using new generation integrated circuits [25] that present high sensitivity ($P_s = -23$ dBm) which almost doubles the read range of the tag, when compared to the results provided in prior scientific publications (e.g., $P_s = -18$ dBm).

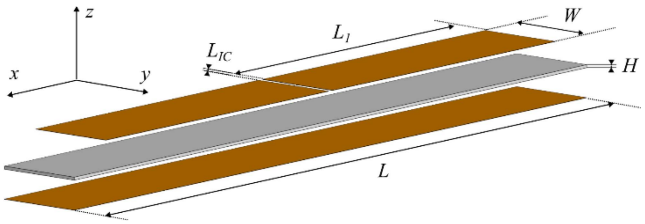

Fig. 2. Exploded-view diagram illustrating the layers and the geometrical parameters of the *D1* wristband antenna design. The values of the geometrical parameters are W=3mm, H=1mm, L=26cm L_1 =11.2 cm and L_{IC} = 2 mm.

III. Wristband Design

The proposed antenna design is intended to maximize the read range of patch-like antennas with specific constraints for wristband inlays, namely low profile (thickness $\leq$ 1 mm) and small width (width $\leq$ 30 mm). The antenna consists of two coupled patches [9], [23], [26], as illustrated in Fig. 2. The patches consist of two metallic strips connected by an RFID integrated circuit. The patches are mounted on a thin plastic substrate, with a conductor layer on the bottom. All copper strips consist of adhesive copper tape with a thickness of 35 μm. The geometrical parameters of the antenna are displayed in Fig. 2.

The intermediate layer consists of a PTFE material with an electrical permittivity of 2.09 and a loss tangent of $2{\cdot}10^{-4}$. These substrate properties were measured using the split post-dielectric resonator technique [27]. The substrate thickness, H, is set to 1 mm. While manufacturers provide different material thickness, thinner substrates reduce the antenna performance considerably by reducing the antenna gain and the tag bandwidth. Both the adhesive copper strips and the PTFE material are flexible, enabling the wristband to be bent around a human wrist.

Once the wristband thickness and width are set to meet the applications constraints, the goal of the antenna design is to find the value of the patch length, L_1, that maximizes the power transfer between the antenna and the microchip in the FCC frequency band. The microchip used in this work is the Alien Higgs-4 [28], with a sensitivity of -20.5 dBm. Specifically, the antenna is designed to achieve complex conjugate impedance matching in the worst-case scenario, where it is bent around the arm and rolled up on itself. Since the structure can be modeled as two open-ended transmission lines in series with the integrated circuit [29], L_1 can be adjusted to modify the antenna input impedance to control the tag complex conjugate impedance matching. This is illustrated in [21, Fig. 3b], showing an approximate frequency shift per millimeter variation of L_1 of 10 MHz, and a deviation of $\sim$8 MHz between simulations and measurements. Taking into consideration these effects, L_1 was finally set to 11.2 cm to account for the overlapping effect that will be introduced in the next section.

In addition, the transmission line-like operation reduces the antenna de-tuning produced by objects in the proximities of the antenna. The proposed layout avoids shorting pins, which simplifies the fabrication process and increases the antenna gain, at the cost of increasing the tag length.

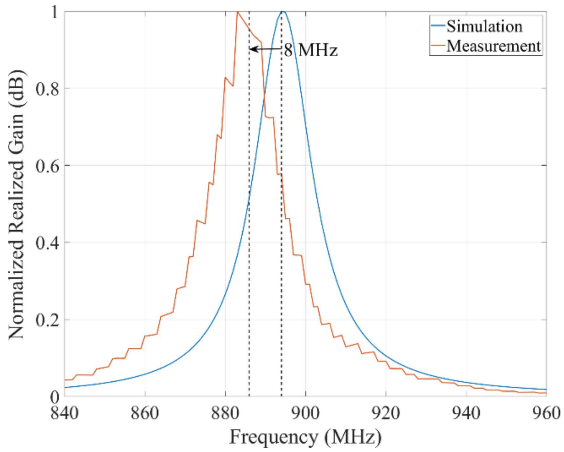

Fig. 3. Normalized realized gain obtained from simulations and measurements for the antenna in free space.

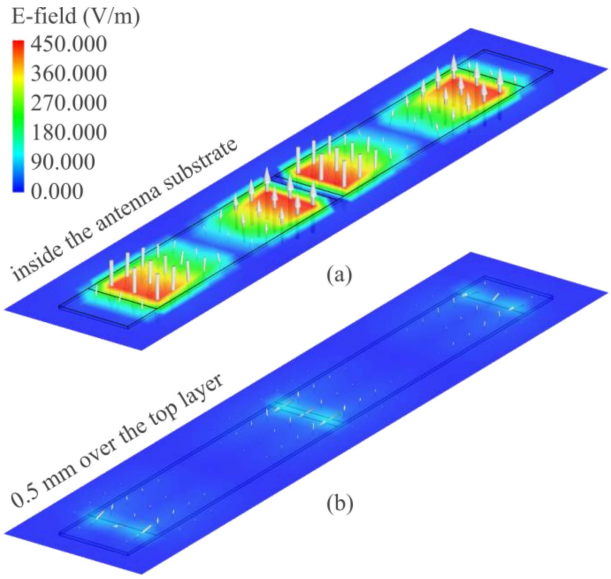

Fig. 4. Near field simulations for planes (a) z = 0.5 mm (within the antenna substrate), and (b) z = 1.5 mm (0.5 mm over the antenna top layer).

The normalized tag realized gain in free space is compared through simulation and measurement results. Simulation values have been obtained using FEKO electromagnetic simulation software [30]. Measurements have been conducted using the Tagformance Pro [31] measurement system. The results in Fig. 3 show good matching between simulations and measurements, with an error smaller than 1%.

Near field simulations are presented in Fig. 4 to validate the patch antenna-like operation. Two different cuts are plotted for values of z = 0.5 mm and 1.5 mm, corresponding to the planes in the middle of the antenna substrate (Fig. 4a) and over the antenna (Fig. 4b), respectively. The electrical field of Fig. 4a on each of the antenna arms resembles the field distribution of a patch antenna (open-ended microstrip transmission line), including the edge radiation at the radiating and non-radiating slots [32], corresponding to the first resonating mode (quasi-TEM mode). Indeed, the fields correspond to a transmission line which length has been made slightly smaller than half

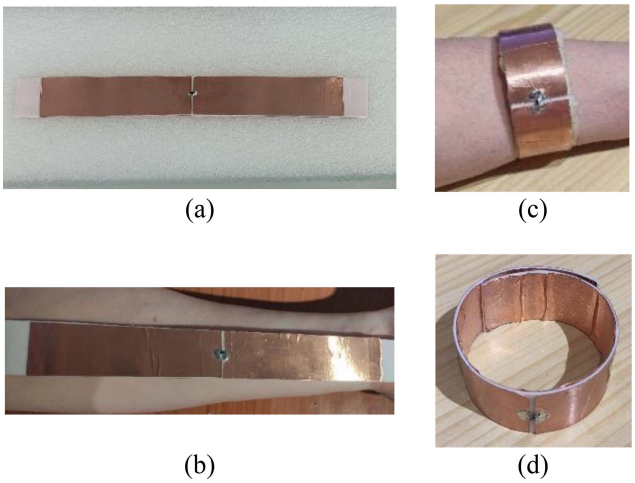

Fig. 5. Images of the wristband in the four studied scenarios: (a) flat configuration in free space, (b) flat configuration over a human arm, (c) wrapped around a human arm without overlapping of the wristband ends, and (d) overlapped wristband with visible wrinkles in the copper tape.

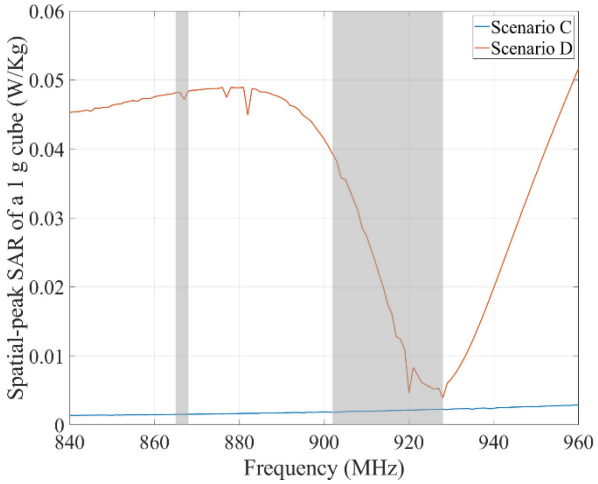

Fig. 6. SAR values computed from simulation on the antenna design overlapped around the arm.

a wavelength, for proper impedance matching. The fringing fields can be observed in the inclination of the electric field arrows with respect to the z axis, at the edges of the patches. The electric field distribution of Fig. 4b shows three areas where the electric field intensity is higher, corresponding with the three radiating slots of the structure. The two slots at the ends are separated from the central slot by a distance close to half a wavelength and, therefore, the fields radiated by all of them contribute in phase to the overall antenna far field radiation.

IV. Performance Analysis

This analysis is intended to understand the cumulative effects that unitary independent modifications of the measurement setup have in the performance of the proposed design. The prototype is fabricated in a flat configuration (Fig. 5a), and then it is bent around a human arm for its utilization. In this process, two events affect the performance of the antenna, namely the proximity of the human arm, and the bending of the wristband, which in this application occur simultaneously. To isolate the effects of both processes, this section analyzes the antenna response in four scenarios. Scenario A consists of a flat antenna configuration in free space (Fig. 5a), Scenario B consists of a flat antenna configuration over a human arm (Fig. 5b), Scenario C consists of an antenna bent over a human arm without overlapping the wristband ends (Fig. 5c), and Scenario D consists of an overlapped antenna configuration (Fig. 5d) wrapped around a human arm.

A. Specific Absorption Rate (SAR)

The SAR limit in the United States is 1.6 W/kg, and 2 W/kg for the European Union. The simulated SAR values of the arm wearing the wristband antenna are presented in Fig. 6 for scenarios C and D. The results show that the SAR is more than 32 times smaller than the permissible limits in the U.S., which is the more restrictive specification, for the worst-case scenario of the overlapped antenna (Scenario D). These findings underscore the effectiveness and safety of the antenna in terms of exposure to electromagnetic radiation, as SAR remains significantly below the thresholds set by both U.S. and European regulations. The European (EU: 865-868 MHz) and the North American (FCC: 902-928 MHz) frequency bands are marked as grey areas in the next figures.

B. Tag Antenna Gain, G_{tag}

Fig. 7 shows the simulated gain pattern for the four scenarios under analysis. In Scenario A, the radiation pattern resembles a toroidal shape, while it's considerably more directive in the direction of the positive z-axis. Placing the antenna over a human arm (Scenario B), the pattern becomes more directive. However, the radiation efficiency decreases due to the losses of the human body, which results in a decrease of more than 4 dB in the main direction. In Scenario C, bending the antenna over the arm has an even stronger effect both in the gain pattern shape and the radiation efficiency. In these circumstances, the antenna presents two main lobes at both sides of the arm, and the maximum antenna gain is reduced by 4 dBs more. In Scenario D, the antenna ends are overlapped. The gain pattern for this setting has again a single main lobe, while the antenna gain is reduced again by 6 dB.

C. Tag Impedance Matching

The same cases are analyzed in terms of the antenna input reactance. Fig. 8 shows the reactance of the antenna in the four scenarios. We can see the deviations in the resonant frequencies. For the flat antenna in free space, the resonant frequency is around 926 MHz, and it barely changes for the flat antenna over the arm. Bending the antenna produces a frequency shift of the resonant frequency to lower frequencies by 6 and 3.5 MHz, for the Scenario C and D, respectively. The negative of the imaginary part of the complex conjugate of the microchip impedance is also plotted as a green line. Thus, when the antenna reactance coincides with the microchip reactance, the power transmission between them is maximum. Fig. 8 shows that, in the flat antenna configurations, the

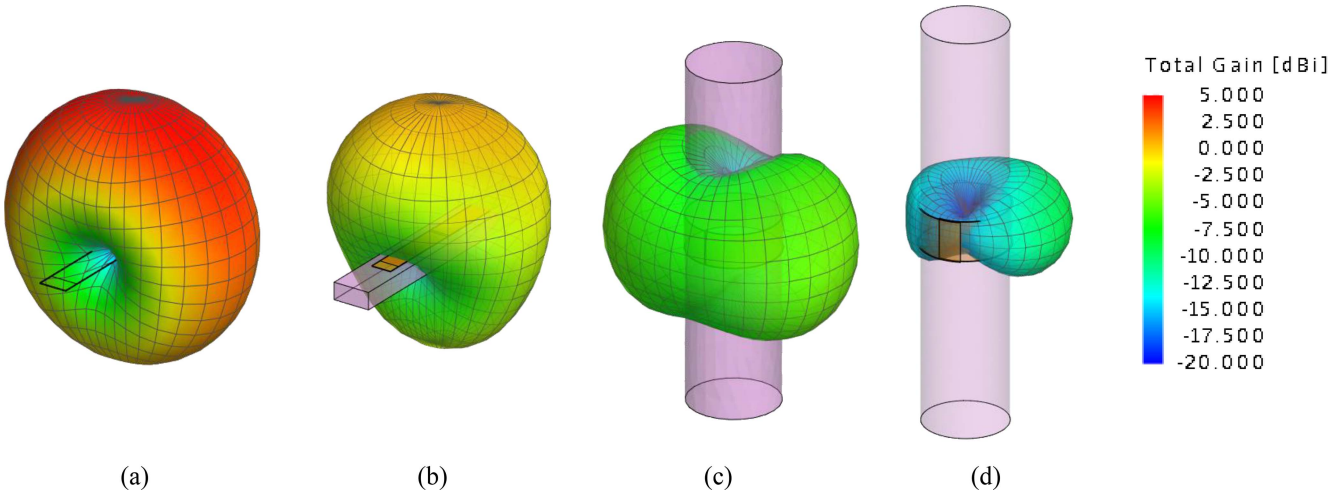

Fig. 7. 3D gain patterns of the proposed antenna in the four scenarios under analysis: (a) flat antenna in free space, (b) flat antenna over a human arm, (c) bent antenna over the human arm, and (d) overlapped antenna around a human arm.

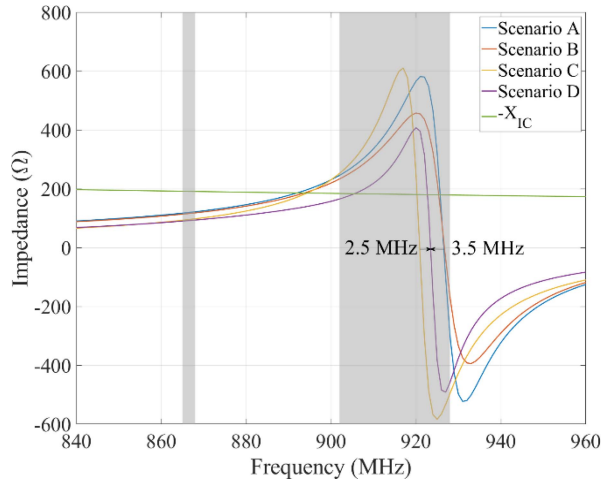

Fig. 8. Plot of the antenna input reactance, in the four studied scenarios, and the reversed sign microchip input reactance.

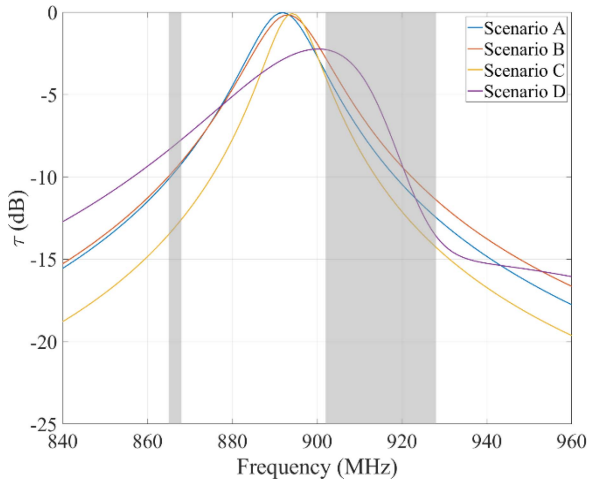

Fig. 9. Power transmission coefficient of the wristband in the four studied scenarios, obtained from simulations.

impedance matching occurs also at close frequencies ($\Delta f < 1$ MHz), caused by the losses due to the presence of the human arm. Equivalently, Fig. 9 shows the values of the power transmission coefficient, τ_{tag}, for these same scenarios. In Scenario D, the impedance matching occurs at a different frequency due to the higher losses of the overlapped antenna.

D. Read Range

Next, the performance of the antenna in terms of the attainable read range will be analyzed. The simulated read range, R_r, has been obtained for an $EIRP_{max} = 3.2$ W, using Equation (1).

$$R_r = \frac{\lambda}{4\pi}\sqrt{\frac{EIRP_{\max} \cdot G_{tag}\tau_{tag}}{P_s}} \tag{1}$$

where λ is the wavelength, P_s is the microchip sensitivity,

Fig. 10 shows the simulated read range obtained for the 4 previous scenarios. As expected, the flat antenna in the free space obtains a considerably high read range, over 25 meters. Then, it decreases to 15 meters for the flat antenna over the arm, 10 meters for the antenna around the arm without overlapping, and 5 meters with overlapping.

The measured read range has been computed using Equation (2). The measurement distance between the reader antenna and the tag, R, is fixed and a power ramp from the reader is applied until the tag responds. $EIRP_{to}$ is the equivalent isotropic radiated power of the first measurement step in which the tag becomes responsive (the microchip turns on).

$$R_r = R\sqrt{\frac{EIRP_{\max}}{EIRP_{to}}} \tag{2}$$

Fig. 11 illustrates the read range measurements for the same configurations, performed with the Tagformance Pro. At first sight, it can be seen that the read ranges from simulations and measurements differ by a factor between 1.5 and 2. This difference can be explained by the deterioration of the prototype materials after bending and unfolding the wristband,

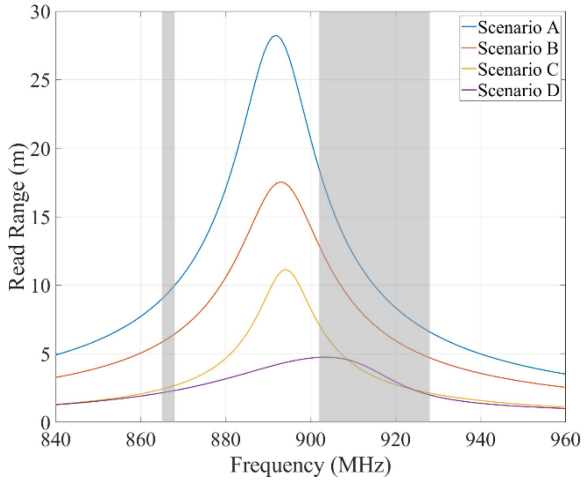

Fig. 10. Read range results for the four cases under analysis, obtained from simulations.

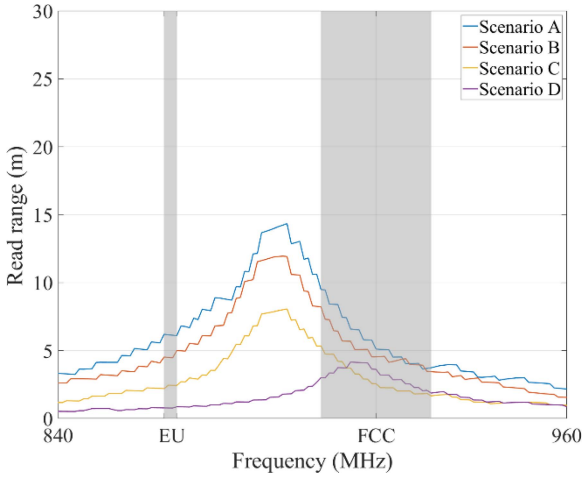

Fig. 11. Read range results for the four cases under analysis, measured with an EIRP=4 W.

which causes wrinkles in the copper strips (see Fig. 5d) that detune the antenna input impedance and increases the losses. The effect has been accounted at simulation time to achieve proper impedance matching, but the losses due to material imperfections, cannot be eliminated. The solution is to improve the fabrication process, and to use different materials in the prototype fabrication. For instance, using copper foils that can be bent to the required extent while keeping the structural integrity, and avoiding inter-layer adhesive materials.

In the last experiment, we measure the read range of the wristband for three different subjects with different wrist perimeters. The results are displayed in Fig. 12. In agreement with Fig. 11, thin wrists are better matched because when wrapping the wristband around the arm overlapping occurs, exactly like in scenario D. In thick wrists the overlapping is smaller or insignificant, like in the case of the wrist with a perimeter of 235 mm, or inexistent, like in the case of the perimeter of 273 mm.

V. Performance Comparison

In this section, the set of commercial wristbands shown in Fig. 13 and the proposed design are characterized through

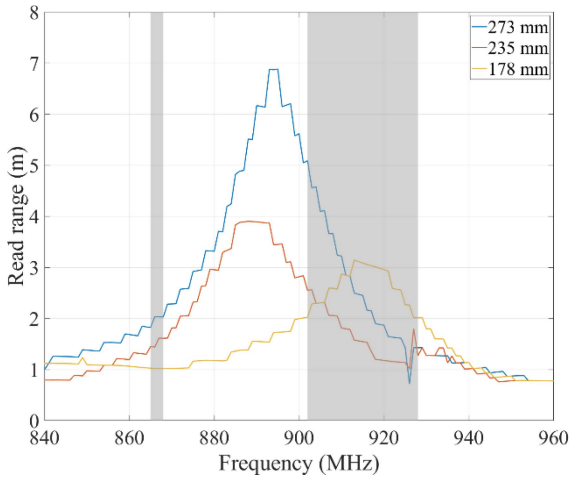

Fig. 12. Read range measurement results for three different wrist sizes: 273 mm, 235 mm and 178 mm.

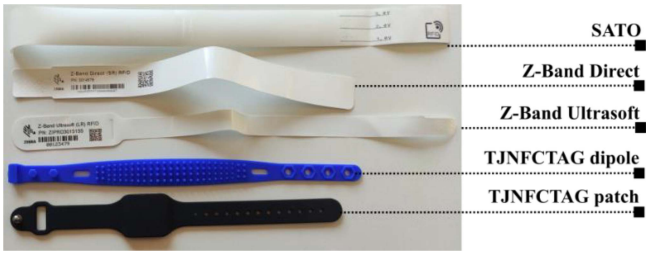

Fig. 13. Image of the set of commercial wristbands selected for the experiment. The devices are tagged, at the right side of the image, with the names used to refer them in the following discussion.

read range measurements, using the Tagformance Pro. The measurement setup is displayed in Fig. 14 for wristbands with the antenna around the human arm (Fig. 14a) and for Flagtag antenna wristbands (Fig. 14b). All wristbands were tightly fastened to the human arm. Fig. 15 shows the results of the read range measurements. All results are computed for a microchip sensitivity of -23 dBm, to discount the effect of the different microchips, according to the Equation (3), where P_{s1} is the sensitivity of the microchip used in the measurements, R_1 is the measured read range, P_{s2} is the new microchip sensitivity the measurement is transformed to, and R_2 is the transformed read range.

$$R_2 = R_1\sqrt{\frac{P_{s1}}{P_{s2}}} \tag{3}$$

The three wristbands on the top of Fig. 13 consist of thermal paper wristbands and the bottom two consist of rubber bands. Thermal paper antennas can also be divided in two groups: wristbands with the antenna placed directly over the human arm, such as the Z-Band Direct [18], and flag tag wristbands, where the antenna is hanging from the human arm to increase the radiation efficiency, such as SATO wristband [17] and Z-Band Ultrasoft [18].

Fig. 15 shows that the lowest read range is achieved by the Z-Band Direct, with only 1 meter of maximum read range. The rubber band embedding a patch antenna attains 5 meters in a small bandwidth inside the FCC band. The rubber band

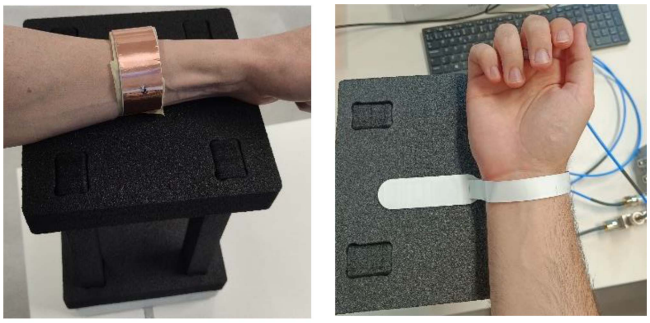

(a) (b)

Fig. 14. Photographs of the measurement setup used during the measurements of (a) the proposed wristband antenna in the Scenario D, and (b) the Z-Band Ultrasoft thermal paper band in the best-case scenario.

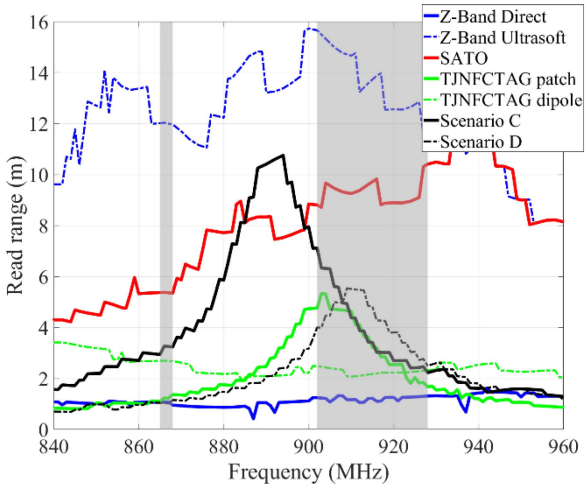

Fig. 15. Read range measurements of the commercial wristbands of Fig. 13 and the proposed one wristband design in the configurations of scenario C and D. These results have been calculated for a microchip sensitivity of −23 dBm in all cases.

with the meander line antenna (TJNFCTAG dipole) reaches over 2 meters in the two main bands. In the case of Flagtag thermal paper wristbands, the displayed measurements results correspond to the best-case scenario. That is when the dipole antenna is totally flat and completely separated from the human arm (Fig. 14b). Under these circumstances the SATO wristband reaches between 5 and 10 meters in the FCC and the ETSI bands. And the Z-Band Ultrasoft reaches read ranges over 12 meters in both bands. In the case of the wristband proposed in this contribution, wristbands for thick arms, like in the case of Scenario C are expected to achieve read ranges over 10 meters for a limited bandwidth, while a tight configuration (Scenario D) attains read ranges over 5 meters.

Thermal paper wristbands embedding the Flagtags obtain the highest performance, but they are also more sensitive to physical stress that can damage the tag, reduce its read range, or even make it unreadable. In addition, these Flagtag antennas can also be put in direct contact with the skin, in which case the read range will be like the Z-Band Direct. Moreover, the manufacturing cost of these devices is very low and thermal paper wristbands can be printed onsite using commercial printers [33]. On the other hand, rubber bands are more robust to physical stress and more reliable under a wider range of events. However, these devices have a higher manufacturing cost, and they attain lower read ranges.

VI. Conclusion

This contribution comprises the performance analysis of the long-range, low-cost, thin, and flexible antenna design for UHF RFID wristbands presented in the IEEE International Conference on RFID Technology and Applications (RFID-TA), held on September 4-6, 2023, Aveiro, Portugal, under the title “A durable and flexible, low-cost tag antenna design for UHF RFID wearable applications”.

The key aspects to highlight are the following: this patch-like design provides significant frequency stability, i.e., it significantly reduces detuning caused by the proximity of lossy material objects. Comparisons between simulations and measurements show that the manufacturing process and materials used in the prototype fabrication are critical to optimize the performance. Therefore, improving the fabrication process and using different materials can have a dramatic impact on the antenna performance, and simulations suggest that the read range can be extended by a factor between 1.5 and 2.

The current performance of the proposed wristband design is compared to the current solutions in the state of the art in Table I. The comparison shows that the proposed design attains higher read ranges with a lower thickness, at the expense of a larger antenna footprint. The prototype has been benchmarked against current commercial solutions, demonstrating performance comparable to that of the best-performing devices. It ensures a read range over 3 meters when used for human identification and tracking. The proposed wristband offers extra robustness than commercial thermal paper wristbands, at the expense of increasing the wristband thickness. And it reduces the costs and provides higher read range than rubber bands. Moreover, the “flat” configuration shows potential for on-body applications that require long read ranges.

References

[1] J. Xu et al., “The principle, methods and recent progress in RFID positioning techniques: A review,” *IEEE J. Radio Freq. Identif.*, vol. 7, pp. 50–63, 2023, doi: 10.1109/JRFID.2022.3233855.

[2] G. Figueiredo, B. Hubbs, and A. D. Radadia, “Monitoring head orientation using passive RFID tags,” *IEEE J. Radio Freq. Identif.*, vol. 7, pp. 582–590, 2023, doi: 10.1109/JRFID.2023.3323948.

[3] A. Mostaccio, G. M. Bianco, G. Marrocco, and C. Occhiuzzi, “RFID technology for food industry 4.0: A review of solutions and applications,” *IEEE J. Radio Freq. Identif.*, vol. 7, pp. 145–157, 2023, doi: 10.1109/JRFID.2023.3278722.

[4] G. M. Bianco et al., “UHF RFID and NFC point-of-care—Architecture, security, and implementation,” *IEEE J. Radio Freq. Identif.*, vol. 7, pp. 301–309, 2023, doi: 10.1109/JRFID.2023.3268422.

[5] C. Feng, J. Xiong, L. Chang, F. Wang, J. Wang, and D. Fang, “RF-identity: Non-intrusive person identification based on commodity RFID devices,” *Proc. ACM Interact. Mob. Wearable Ubiquitous Technol.*, vol. 5, no. 1, pp. 1–23, Mar. 2021, doi: 10.1145/3448101.

[6] B. Siregar, S. Efendi, C. Setiawan, and F. Fahmi, “RFID wristband for motorbikes real-time security system,” in *Proc. 3rd Int. Conf. Electr., Telecommun. Comput. Eng. (ELTICOM)*, Medan, Indonesia, 2019, pp. 116–119, doi: 10.1109/ELTICOM47379.2019.8943903.

[7] S.-W. Jiang, S.-Y. Chen, W.-E. Chen, and H.-T. Wu, “Development of personnel epidemic prevention monitoring access control system,” in *Proc. Int. Comput. Symp.*, Singapore, 2022, pp. 223–229, doi: 10.1007/978-981-19-9582-8_20.

[8] F. Ebrahimzadeh, E. Nabovati, M. R. Hasibian, and S. Eslami, "Evaluation of the effects of radio-frequency identification technology on patient tracking in hospitals: A Systematic review," *J. Patient Saf.*, vol. 17, no. 8, pp. e1157–e1165, Dec. 2021, doi: 10.1097/PTS.0000000000000446.

[9] S. Lopez-Soriano and J. Parron, "Low profile UHF RFID tag for wristbands in healthcare applications," in *Proc. 8th Eur. Conf. Antennas Propag. (EuCAP)*, The Hague, The Netherlands, 2014, pp. 874–877, doi: 10.1109/EuCAP.2014.6901901.

[10] S. Lopez-Soriano and J. Parron, "Wearable RFID tag antenna for healthcare applications," in *Proc. IEEE APS Topical Conf. Antennas Propag. Wireless Commun. (APWC)*, Torino, Italy, 2015, pp. 287–290, doi: 10.1109/APWC.2015.7300156.

[11] S. Lopez-Soriano and J. Parron, "Design of a small-size, low-profile, and low-cost normal-mode helical antenna for UHF RFID wristbands," *Antennas Wireless Propag. Lett.*, vol. 16, pp. 2074–2077, 2017, doi: 10.1109/LAWP.2017.2696300.

[12] G.-L. Huang, C.-Y.-D. Sim, S.-Y. Liang, W.-S. Liao, and T. Yuan, "Low-profile flexible UHF RFID tag design for wristbands applications," *Wireless Commun. Mobile Comput.*, vol. 2018, pp. 1–13, Jun. 2018, doi: 10.1155/2018/9482919.

[13] A. Mehmood, X. Chen, H. He, S. Ma, L. Ukkonen, and J. Virkki, "Intelligent wristbands-fabrication of wearable RFID solutions by 3-D printing pen," in *Proc. IEEE Int. Symp. Antennas Propag. North Am. Radio Sci. Meet.*, Montreal, QC, Canada, 2020, pp. 1319–1320, doi: 10.1109/IEEECONF35879.2020.9329572.

[14] L. Catarinucci, F. P. Chietera, and R. Colella, "Permittivity-customizable ceramic-doped silicone substrates shaped with 3-D-printed molds to design flexible and conformal antennas," *IEEE Trans. Antennas Propagat.*, vol. 68, no. 6, pp. 4967–4972, Jun. 2020, doi: 10.1109/TAP.2020.2969748.

[15] N. S. Khamaruzaman, M. Jusoh, T. Sabapathy, M. N. Osman, S. Subahir, and M. H. Jamaluddin, "Wearable UHF RFID antenna based metamaterial," in *Proc. IEEE Asia Pac. Conf. Appl. Electromagnet. (APACE)*, Penang, Malaysia, 2021, pp. 1–5, doi: 10.1109/APACE53143.2021.9760582.

[16] "TJNFCTAG RFID wristbands." Accessed: Feb. 21, 2022. [Online]. Available: https://www.tjnfctag.com/product-category/custom-rfid-wristband/

[17] *SATO RFID Wristbands*, Satoeurope, Heidelberg, Germany. Accessed: Feb. 21, 2024. [Online]. Available: https://www.satoeurope.com/products/wristbands.php

[18] *Z-Band UHF RFID Wristband*, Zebra, Lincolnshire, U.K., Accessed: Feb. 21, 2022. [Online]. Available: https://www.zebra.com/content/dam/zebra_new_ia/en-us/solutionsverticals/product/Supplies/rfid/z-band/spec-sheet/z-band-rfid-wristband-specsheet-en-us.pdf

[19] A. Mehmood et al., "Body movement-based controlling through passive RFID integrated into clothing," *IEEE J. Radio Freq. Identif.*, vol. 4, no. 4, pp. 414–419, Dec. 2020, doi: 10.1109/JRFID.2020.3010717.

[20] F. Camera et al., "Monitoring of temperature stress during firefighters training by means of RFID epidermal sensors," in *Proc. IEEE Int. Conf. RFID Technol. Appl. (RFID-TA)*, Pisa, Italy, 2019, pp. 499–504, doi: 10.1109/RFID-TA.2019.8892269.

[21] S. López-Soriano, J. Melià-Seguí, and J. Parrón, "A durable and flexible, low-cost tag antenna design for UHF RFID wearable applications," presented at the Int. Conf. RFID Technology and Applications (RFID-TA), Aveiro, Portugal., 2023, pp. 9–12.

[22] G. Marrocco, "The art of UHF RFID antenna design: Impedance-matching and size-reduction techniques," *IEEE Antennas Propag. Mag.*, vol. 50, no. 1, pp. 66–79, Feb. 2008, doi: 10.1109/MAP.2008.4494504.

[23] S. Lopez-Soriano and J. Parron, "Performance assessment of a novel miniaturized RFID tag for inventorying and tracking metallic tools," *IEEE J. Radio Freq. Identif.*, vol. 2, pp. 127–133, 2018, doi: 10.1109/JRFID.2018.2868780.

[24] "AD midas flagtag." Accessed: Feb. 21, 2024. [Online]. Available: https://rfid.averydennison.com/en/home/product-finder/midas-flagtag.html

[25] "NXP UCODE 8." Accessed: Feb. 21, 2024. [Online]. Available: https://www.nxp.com/products/rfid-nfc/ucode-rain-rfid-uhf/ucode-8-8m:SL3S1205-15

[26] M. Polivka and M. Svanda, "Stepped impedance coupled-patches tag antenna for platform-tolerant UHF RFID applications," *IEEE Trans. Antennas Propagat.*, vol. 63, no. 9, pp. 3791–3797, Sep. 2015, doi: 10.1109/TAP.2015.2447034.

[27] J. Krupka, R. N. Clarke, O. C. Rochard, and A. P. Gregory, "Split post dielectric resonator technique for precise measurements of laminar dielectric specimens-measurement uncertainties," in *Proc. 13th Int. Conf. Microw., Radar Wireless Commun. (MIKON)*, Wroclaw, Poland, 2000, pp. 305–308, doi: 10.1109/MIKON.2000.913930.

[28] "Alien Higgs-4 integrated circuit," Datasheet, Radio Freq. Identificat., Cranberry PA, USA, Accessed: Feb. 21, 2024. [Online]. Available: https://www.alientechnology.com/products/ic/higgs-4/

[29] J. P. S. López-Soriano, "Small UHF RFID tag antenna for metallic objects," in *Proc. 9th Eur. Conf. Antennas Propag. (EuCAP)*, Lisbon, Portugal, 2015, pp. 1–5.

[30] "FEKO," Accessed: Feb. 21, 2024. [Online]. Available: https://www.altair.com.es/feko/

[31] *Tagformance® Pro*, Voyantic, Helsinki, Finland. Accessed: Feb. 21, 2024. [Online]. Available: https://voyantic.com/lab/tagformance-pro/

[32] C. A. Balanis, *Antenna Theory: Analysis and Design*, 4th ed. Hoboken, NJ, USA: Wiley, 2016.

[33] "RFID PRINTERS." Accessed: Feb. 21, 2024. [Online]. Available: https://www.zebra.com/us/en/products/rfid/rfid-printers.html

Sergio López-Soriano received the M.Sc. degree in micro and nanoelectronics engineering and the Ph.D. degree in electronics and telecommunication engineering from the Universitat Autonoma de Barcelona, Bellaterra, Spain, in 2013 and 2018, respectively. He was enrolled in the Scatterer ID Project with LCIS Laboratoire from 2018 to 2019, and the Ubiquitous Computing Lab, Universitat Pompeu Fabra from 2019 to 2022, as a Postdoctoral Researcher. He is currently with the WiNe Group, Universitat Oberta de Catalunya, Barcelona, Spain. And, he is an Associate Lecturer with the Universitat Autònoma de Catalunya. His current research interests include radio frequency sensors, embedded systems, and antenna design.

Joan Melià-Seguí (Senior Member, IEEE) received the B.Sc. and M.Sc. degrees in telecommunication engineering from the Universitat Politècnica de Catalunya, and the Ph.D. degree from the Universitat Oberta de Catalunya (UOC). He has been a Researcher with Universitat Pompeu Fabra, a Visiting Researcher with the Palo Alto Research Centre (Xerox PARC), and a Fulbright Visiting Scholar with the Massachusetts Institute of Technology. He is currently an Associate Professor with the Faculty of Computer Science, Multimedia and Telecommunication Engineering, UOC. He has authored over 40 technical peer-reviewed publications. His research interests include sustainability and low-cost RF sensing.

Josep Parrón Granados was born in Sabadell, Spain, in 1970. He received the M.S. degree in telecommunication engineering and the Ph.D. degree from the Universitat Politècnica de Catalunya (UPC), Spain, in 1994 and 2001, respectively.

From 2000 to 2002, he was an Assistant Professor with the Electromagnetic and Photonic Engineering Group, Signal Theory and Communication Department, UPC. Since 2002, he has been a Lecturer with the Telecommunication and Systems Engineering Department, Universitat Autònoma de Barcelona, Spain. He has coauthored 34 technical peer-reviewed journal papers and over 90 conference contributions. His current research interests include numerical methods for electromagnetism, antenna analysis and design, phased arrays, and reflective intelligent surfaces.